# Electronic Structure and Low-Lying Electronic States of Al₃O and Al₃O⁻: Photoelectron Spectrum of Al₃O⁻

**Tapan K. Ghanty[†] and Ernest R. Davidson***

*Department of Chemistry, Indiana University, Bloomington, Indiana 47405*

*Received: November 30, 1998; In Final Form: February 8, 1999*

We have calculated the equilibrium geometries of the ground electronic state of $Al_3O$ and $Al_3O^-$ using Hartree−Fock, density functional, and coupled-cluster doubles methods. These molecules are nominally equilateral triangles of Al atoms with an oxygen in the center which distort due to the Jahn−Teller effect. The calculated global minima had $C_{2v}$ symmetry with $(b_2)^1$ $^2B_2$ and $(b_2)^2$ $^1A_1$ configurations, respectively. The global minimum of the lowest triplet state of $Al_3O^-$ was found to have $D_{3h}$ symmetry with an $(e')^2$ $^3A_2'$ electron configuration. While this was the lowest energy state of the molecule among $D_{3h}$ symmetry points, this triplet minimum had slightly higher energy than the $^1A_1$ state at its $C_{2v}$ global minimum. The $^1A_1$ $(a_1)^2$ and the $^1B_2$ $(b_2)^1(a_1)^1$ configurations of $Al_3O^-$ and the $^2A_1$ $(a_1)^1$ configuration of $Al_3O$ lead to transition states of $C_{2v}$ symmetry on the respective potential energy surfaces for pseudorotation. Using the CCD geometries of $(b_2)^2$ $^1A_1$ and $(e')^2$ $^3A_2'$ $Al_3O^-$, configuration interaction calculations have been performed to determine the low-lying vertical excited states of $Al_3O$, and those results have been utilized to interpret the recently reported experimental photoelectron spectrum of $Al_3O^-$. On the basis of the present CI results, new assignments have been made for some of the peaks.

## Introduction

Electron correlation plays an important role for a detailed understanding of the electronic structure of atoms and molecules. The correlation energy, defined as the difference between the nonrelativistic exact energy and the Hartree−Fock energy, is very small compared to the Hartree−Fock energy. The change in correlation energy in a chemical process is usually of the same order of magnitude as the energy differences of chemical interest. Apart from the effect on energy, electron correlation effects are also manifested in the intensity of the photoelectron spectrum of atoms and molecules.

One direct experimental method for obtaining electron binding energy for each orbital is photoelectron spectroscopy (PES). The interpretation of photoelectron spectra has benefited tremendously from simple molecular orbital (MO) models like Hartree−Fock theory, which has been successful in accounting for the main features of photoelectron spectra, especially in the outer valence region. Generally, there is a one-to-one correspondence between the valence molecular orbitals and main ionization peaks. However, simple MO theory cannot account for the lower intensity "extra" peaks that are very often observed.[1] These extra peaks are called "correlation peaks" (although they are also referred to as satellite peaks, shake-up peaks, or many-body peaks), and have zero intensity in the Hartree−Fock model. It is precisely from the effect of electron correlation in atomic or molecular systems that these peaks gain intensity and appear in the photoelectron spectra. Recent benchmark configuration interaction (CI) calculations[2−6] have been able to interpret and predict the electron binding energy spectra of a number of molecular systems. Besides CI, Green's

function methods have also been used extensively[7] to explain the observed photoelectron spectra of molecules.

In recent years, metal clusters have been the subject of several experimental and theoretical investigations[8,9] to understand the electronic structure and bonding, not only for the ground electronic state but also for the low-lying excited electronic states. Due to the likely presence of a large number of closely spaced excited states, it is rather a challenging job to provide a list of the excited states in correct energy order. "Hypermetallic molecules" involving metal stoichiometries exceeding normal valence expectations are now well documented experimentally[9] and have been extensively studied theoretically.[10−12] These species can be regarded as metal clusters bound ionically to a centrally located nonmetallic atom.

Within this class of molecules, $Al_3O$ has been studied both experimentally[10−12] and theoretically.[13−17] Very recently, the photoelectron spectrum of $Al_3O^-$ has also been reported[18] at several photon energies. Although the ground state of neutral $Al_3O$ has been studied theoretically before,[13] to our knowledge there is no theoretical report on the ground state of $Al_3O^-$ or on excited states of $Al_3O$. In order to understand the features in the experimental photoelectron spectrum of $Al_3O^-$, one should have reliable theoretical results for many electronic states of $Al_3O$ and also for all thermally accessible states of $Al_3O^-$. The purpose of this work is to calculate the ground-state geometry of $Al_3O^-$, and the electronic structures and the energies of the low-lying excited states of $Al_3O$ in order to interpret the experimentally observed photoelectron spectrum. Because of complications caused by Jahn−Teller effects (see Results section) computational methods appropriate for degenerate biradicals must be used.

## Theoretical Methods

The geometries of neutral and anionic $Al_3O$ were optimized employing ROHF (restricted open shell Hartree−Fock), TCSCF

---

**TABLE 1: Calculated Bond Lengths and Bond Angles of Low-Lying Electronic States of Al₃O and Al₃O⁻ by Different Methods[a]**

| method | state | $R_1$ | $R_2 = R_3$ | $\theta_1$ | energy ($E_h$) | $\Delta E$ (kcal/mol) |
|---|---|---|---|---|---|---|
| | | | Al₃O | | | |
| ROHF/6-31+G* | $^2B_2$ | 2.001 | 1.800 | 151.6 | −800.638 796 | 0. |
| ROHF/6-31+G* | $^2A_1$ | 1.764 | 1.918 | 96.0 | −800.639 073 | −0.17 |
| UB3LYP/6-31+G* | $^2B_2$ | 1.992 | 1.835 | 163.0 | −802.591 550 | 0. |
| UB3LYP/6-31+G* | $^2A_1$ | 1.780 | 1.950 | 91.9 | −802.587 225 | 2.71 |
| UCCD/6-31+G* | $^2B_2$ | 1.985 | 1.829 | 156.8 | −800.996 762 | 0. |
| UCCD/6-31+G* | $^2A_1$ | 1.780 | 1.939 | 91.8 | −800.996 542 | 0.14 |
| UCCSD(T)/6-31+G* | $^2B_2$ | | | | −801.018 057 | 0. |
| UCCSD(T)/6-31+G* | $^2A_1$ | | | | −801.016 464 | 1.00 |
| | | | Al₃O⁻ | | | |
| TCSCF/6-31+G* | $^1A_1(b_2{}^2)$ | 1.959 | 1.811 | 170.8 | −800.652 661 | 0. |
| TCSCF/6-31+G* | $^1A_1(a_1{}^2)$ | 1.720 | 1.948 | 92.2 | −800.642 288 | 6.51 |
| ROHF/6-31+G* | $^3A_2'(e'^2)$ | 1.844 | 1.844 | 120.0 | −800.649 131 | 2.21 |
| ROHF/6-31+G* | $^1B_2(a_1b_2)$ | 1.909 | 1.833 | 104.1 | −800.638 022 | 9.19 |
| B3LYP/6-31+G* | $^1A_1(b_2{}^2)$ | 2.012 | 1.835 | 177.1 | −802.629 547 | 0. |
| B3LYP/6-31+G* | $^1A_1(a_1{}^2)$ | 1.735 | 1.987 | 87.1 | −802.606 521 | 14.45 |
| UB3LYP/6-31+G* | $^3A_2'(e'^2)$ | 1.866 | 1.866 | 120.0 | −802.612 797 | 10.51 |
| CCD/6-31+G* | $^1A_1(b_2{}^2)$ | 1.999 | 1.828 | 177.5 | −801.023 210 | 0. |
| CCD/6-31+G* | $^1A_1(a_1{}^2)$ | 1.735 | 1.970 | 87.2 | −801.006 308 | 10.61 |
| UCCD/6-31+G* | $^3A_2'(e'^2)$ | 1.860 | 1.860 | 120.0 | −801.012 581 | 6.67 |
| CCSD(T)/6-31+G* | $^1A_1(b_2{}^2)$ | | | | −801.047 152 | 0.00 |
| CCSD(T)/6-31+G* | $^1A_1(a_1{}^2)$ | | | | −801.027 830 | 12.12 |
| UCCSD(T)/6-31+G* | $^3A_2'(e'^2)$ | | | | −801.031 559 | 9.78 |

[a] For each method energy difference calculated with relative to the $^2B_2$ and $^1A_1(b^2)$ state energies of Al₃O and Al₃O⁻, respectively. CCSD(T) energies are calculated at the corresponding CCD optimized geometries. All structures have $C_{2v}$ symmetry with the oxygen near the center of a triangle formed by the aluminum atoms. $R_1$ is the unique Al1O distance while $R_2$ and $R_3$ are the Al2O and Al3O distances. $\theta$ is the unique Al2OAl3 angle while Al1OAl3 and Al2OAl3 define $\theta_2$ and $\theta_3$ which are each $180° − \theta/2$.

(two-configuration self-consistent field), density functional theory (DFT) with B3LYP (three-parameter Becke exchange and Lee−Yang−Parr correlation), and the coupled-cluster doubles (CCD) methods with the 6-31+G* basis set. For DFT and CCD calculations, the Gaussian 94[19] program was used, whereas for ROHF and TCSCF calculations, the HONDO[20] program was used. Utilizing these optimized geometries, CI calculations were performed using the MELD[21] program. The basis set used for the CI calculation is aug-cc-pVTZ excluding the $f$ function and augmenting $d$ function.[22] This basis set is motivated by the need to represent all Al₃O states up to an excitation energy of about 10 eV with CI calculations that are still computationally affordable. The starting orbitals for CI wave functions were obtained from ground state Al₃O⁻ ROHF computations. The canonical virtual orbitals are converted to K orbitals[23] to carry out the CI calculations. The 1$s$, 2$s$, and 2$p$ electrons of aluminum and 1$s$ electrons of oxygen were kept frozen as the core and the remaining valence electrons were treated explicitly in the CI calculations.

Within a closed-shell Hartree−Fock approximation, an $N$-electron molecule can be represented as $\Psi_{HF}(N)$ (the ground state wave function). A primary hole configuration $\Psi_k(N−1)$ (which corresponds to removal of an electron from the $k$th occupied orbital) can be written as $\Psi_k(N − 1) = a_k\Psi_{HF}(N)$, where $a_k$ is an annihilation operator that destroys orbital $k$ in $\Psi_{HF}(N)$. According to Koopmans' theorem, the position of the peaks corresponding to the $n$ occupied orbitals will be given by the negative of their orbital energies. However, as mentioned before, the independent particle model is not adequate to explain the appearance of correlation peaks in photoelectron spectra. There can be excitations followed by ionization, like 1$p$−2$h$ (one particle−two holes), 2$p$−3$h$ (two particles-three holes), etc. Therefore, the wave functions for the ground state of the neutral, $\Psi(N)$, or any state of the ion, $\Psi_k(N−1)$, are written as linear combinations of all possible configurations in the CI method.

The pole strength or intensity of the transition for the $k$th ionic state is defined as

$$S_k{}^2 = ||\langle\Psi_k(N − 1)|\Psi(N)\rangle_{N−1}||^2$$

where the integration is performed over $N − 1$ electrons. The pole strength of the peak corresponding to the 0$p$−1$h$ (primary peak) ionic state configuration will be close to unity and the pole strengths of the peaks associated with other configurations (1$p$−2$h$, 2$p$−3$h$, etc.) are usually very small ($S_k{}^2 \ll 1$). The photoelectron peak intensities are proportional to the pole strength multiplied by the squares of transition moments between the bound orbital and the continuum.

For open-shell initial and final states, the intensities must be averaged over degenerate initial states and summed over degenerate final states; i.e., the weight $w$ of the transition in the system is given by

$$w = \sum_{initial}\sum_{final}S_{if}{}^2/g$$

where $g$ is the degeneracy of the initial state. For the simplest possible open-shell wave functions formed by symmetry-determined linear combinations of Slater determinants using spin and symmetry-constrained orbitals, the sum of $w$ would still be the number of active electrons when summed over all roots of the CI matrix.

## Results

The calculated ground state geometrical parameters and energies for Al₃O and Al₃O⁻ are reported in Table 1. Figure 1 shows the orbital energies and labels for Al₃O⁻. Bonding in these molecules is quite unusual. They are most simply considered to have three Al⁺ ions arranged in an equilateral triangle and attached to a central O²⁻ by coordinate covalent bonds between oxygen $sp^2$ lone pairs and empty Al $p\sigma$ orbitals.
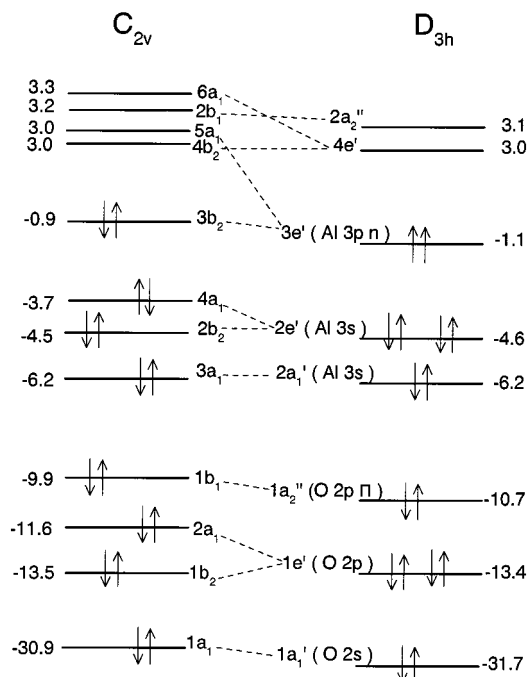
**Figure 1.** Orbital energy (eV) diagram for Al$_3$O$^-$ $3b_2^2$ $^1A_1$ and $3e'^2$ $^3A'_2$ states.



**Figure 2.** Plot indicating the regions of different electronic wave function symmetry on the ground state potential energy surface of Al$_3$O$^-$. Location of minima (MIN) and transition states (TS) are indicated along with the monkey saddle (MS). The stationary points for neutral Al$_3$O are also indicated by +. The TSs are each a relative minimum in this plane with an imaginary frequency for a $b_2$ normal mode.

The Al is essentially unhybridized. The remaining two electrons of Al$_3$O$^-$ (or remaining one electron of Al$_3$O) are placed in an $e'$ (in $D_{3h}$ symmetry) linear combination of $pn$ Al atomic orbitals ($p$ orbitals in the plane but orthogonal to the Al–O bond). The remaining $p\pi$ electron pair of O$^{2-}$ participates to some extent also in coordinate covalent bonding with the empty $p\pi$ orbitals of Al and is the only occupied out-of-plane molecular orbital.

This model predicts that Al$_3$O should have a $e'$ $^2E'$ ground state. This is subject to Jahn–Teller distortion. The simplest result would be distortion to a $C_{2v}$ shape with distortion in one direction leading to a minimum and distortion in the opposite direction leading to a transition state for pseudorotation. That is, one of these points would have all real frequencies and the other would have one imaginary frequency for a normal mode that broke $C_{2v}$ symmetry. Since Al$_3$O has two $e'$ vibrational modes, one associated with angle bending and one with bond stretching, the picture is a little more complicated. As is easily shown,[24] one linear combination of these normal modes will be Jahn–Teller active and the other combination will be inactive. For the neutral molecule, it turns out that the active mode simultaneously stretches the Al–O bond to the unique atom (in $C_{2v}$ symmetry) and opens the angle opposite that atom. Figure 2 depicts this situation for Al$_3$O. Along the positive phase of this distortion the ground state wave function is the $^2B_2$ component of the $^2E'$ state, while along the negative phase the lowest state is the $^2A_1$ component. It is not possible, a priori, to say which of these distortions will lead to the minimum and which to the transition state.

From Table 1, one can see that for Al$_3$O, the $^2A_1$ form with a negative phase of distortion (decrease of the unique bond length and opposite angle) is predicted to be the minimum with ROHF calculations. With better methods like UB3LYP and CCSD(T) (coupled-cluster for single and double excitations and perturbation treatment of triple excitations), the positive phase of distortion with a $^2B_2$ wave function gives the lower energy. The nature of these stationary points was confirmed by frequency calculations. These findings are consistent with earlier
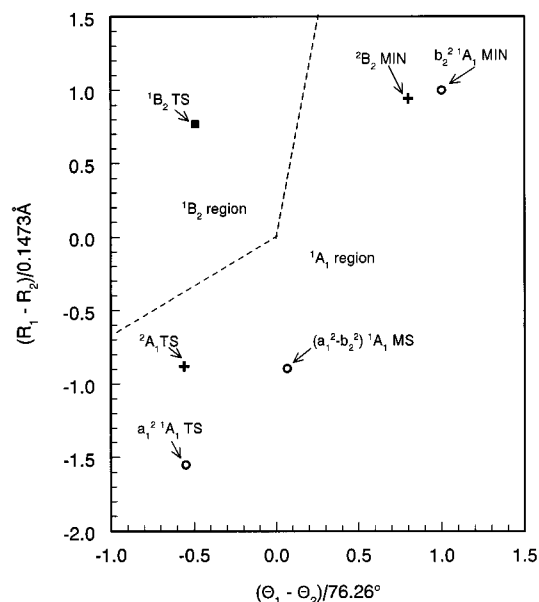
results[13] in which UHF/6-31G* gave a negative distortion with a $^2A_1$ global minimum while UMP2/6-31G* calculations gave a positive phase and a $^2B_2$ wave function at the global minimum.

The valence electron configurations (core orbitals are not included in the numbering scheme) for the $^2B_2$ and $^2A_1$ structures have been found to be ...$(4a_1)^2(2b_2)^2(3b_2)^1$ and ...$(4a_1)^2(2b_2)^2$-$(5a_1)^1$, respectively. It is to be noted that in the paper by Boldyrev and Schleyer,[13] the electron configurations for both the $^2B_2$ and $^2A_1$ states were reported incorrectly as ...$(4a_1)^2(2b_1)^2$-$(2b_2)^1$ and ...$(4a_1)^2(2b_1)^2(5a_1)^1$. This is just a transcription error, however, as we have verified their numerical results using the correct configuration. On the other hand, Wu et al.[18] based their assignment of the photoelectron spectrum of Al$_3$O$^-$ on this mistyped configuration for Al$_3$O.

From Table 1, one can compare the energy difference between the $^2B_2$ and $^2A_1$ states of neutral Al$_3$O. With the ROHF method and a 6-31+G* basis, the $^2A_1$ state is found to be more stable by 0.2 kcal/mol, whereas with UB3LYP, CCD, and CCSD(T) methods, the $^2B_2$ state is found to be more stable by 2.7, 0.1, and 1.0 kcal/mol, respectively. It is interesting to compare the present results with earlier reported[13] energy differences of 1.4 kcal/mol with $^2A_1$ more stable (UHF/6-31G*), compared to 1.1 kcal/mol (UMP2/6-31G*) and 0.5 kcal/mol (UMP4/6-311+G*) with $^2B_2$ more stable. In the present work, we have not considered the $D_{3h}(^2E)$ structure for the neutral Al$_3$O as it has been found[13] to be a high energy structure.

For Al$_3$O$^-$, so far there has not been any experimental or theoretical report on the geometry or the electronic structure. Following the same reasoning as for Al$_3$O, we would expect four low-energy wave functions at a $D_{3h}$ geometry with $e'^2$ configuration. Hund's rule suggests the lowest state should be $^3A_2'$. In the notation of the orbitals after $C_{2v}$ distortion, the next two wave functions would be the $^1(a_1b_2)$ and $(a_1^2 - b_2^2)$ components of a $^1E'$ state. Finally, there would be a higher energy $^1A_1'$ state with configuration $(a_1^2 + b_2^2)$. Notice that none of these singlet states can be properly described by one Slater determinant. All are biradicals and require a multireference

starting point. The minimum description is a two-electron/two-orbital CASSCF (complete active space SCF). For the $^1(a_1 b_2)$ wave function this is an open-shell singlet ROHF function, while for the $(a_1^2 - b_2^2)$ function a TCSCF (two configuration SCF) calculation is required. No single reference method such as DFT or CCD is appropriate for these states.

As before, the $^1E'$ state is subject to Jahn−Teller distortion. Using the TCSCF and ROHF methods, we have calculated several points of the lowest energy potential energy surface of $Al_3O^-$ and plotted the results in Figure 2 as $(R_1 - R_2)$ vs $(\theta_1 - \theta_2)$, where $R_1$ is the bond length of the unique Al−O bond (in $C_{2v}$ symmetry) and $\theta_1$ is the unique bond angle, and $R_2$ and $\theta_2$ are the other bond lengths and bond angles, respectively. Figure 2 divides the $C_{2v}$ distortion plane into a region where the lowest singlet state is $^1B_2$ and a region where it is $^1A_1$. In the case of $Al_3O^-$, the Jahn−Teller active mode is now stretch of the unique bond with simultaneous compression of the opposite angle. The positive phase of this distortion leads to a $^1B_2$ wave function for the lowest energy singlet state while the opposite phase leads to $^1A_1$. Along the dividing line between the $^1A_1$ and $^1B_2$ regions the energy is degenerate. This line is the locus of a branch cut in the potential energy surface.[24] When all six internal coordinates are considered, this branch-out is seen to be four-dimensional.

We have found that the $^1A_1$ configuration gives the global minimum of $Al_3O^-$. This is found to have $C_{2v}$ symmetry and the TCSCF wave function is mostly ...$(4a_1)^2(2b_2)^2(3b_2)^2$ with only a small amount of ...$(4a_1)^2(2b_2)^2(5a_1)^2$. As Figure 2 shows, this $^1A_1$ minimum is not simply the opposite phase distortion from the $^1B_2$ transition state. This is an interesting illustration of a so-called pseudo-Jahn−Teller effect. After $C_{2v}$ distortion, the $(a_1^2 - b_2^2)$ and $(a_1^2 + b_2^2)$ $D_{3h}$ wave functions have the same $C_{2v}$ symmetry and can be strongly mixed by $C_{2v}$ distortions. This effect is often invoked to explain the existence of broken symmetry double minima, as in the rectangular distortion of cyclobutadiene.[25] In the case of $Al_3O^-$, it appears that this mixing is strongest in the combination of bond stretching and angle distortions orthogonal to the one that is Jahn−Teller active. After distortion in this mode, there are two $^1A_1$ stationary points. At one, the wave function is predominantly $a_1^2$ and at the other it is $b_2^2$. The $b_2^2$ stationary point is found to be a true minimum while the $a_1^2$ stationary point has one imaginary frequency for a normal mode that breaks the $C_{2v}$ symmetry. Based on these TCSCF results, it appears that a single reference SCF or DFT calculation should produce a reasonable result in the neighborhood of the $b_2^2$ $^1A_1$ minimum. It is interesting to note that the $Al_3O^-$ $^1A_1$ $(b_2)^2$ and $^1A_1$ $(a_1)^2$ stationary point geometries are close to the corresponding neutral $Al_3O$ $^2B_2$ $(b_2)^1$ and $^2A_1$ $(a_1)^1$ stationary point geometries, respectively. These two $^1A_1$ stationary points in Figure 2 are connected by a monkey saddle which has two imaginary frequencies. One of these frequencies is for the $b_2$ normal mode that destroys $C_{2v}$ symmetry while the other is for an $a_1$ normal mode connecting the $a^2$ and $b^2$ $^1A_1$ stationary points. At the monkey saddle, the wave function is nearly $(a_1^2 - b_2^2)$.

We have also considered the first triplet state of $Al_3O^-$ and have found that it has a global minimum at a $D_{3h}$ geometry with the ...$(2e')^4(3e')^2$ $^3A_2'$ configuration. All the calculated vibrational frequencies are real for this triplet minimum. This triplet minimum is slightly higher in energy than the $b_2^2$ $^1A_1$ minimum energy $C_{2v}$ structure. This is not a violation of Hund's rule since the triplet state is the lowest energy state at its $D_{3h}$ minimum. It can be noticed from Table 1 that for $Al_3O^-$, the relative energy order at the stationary points is $^1A_1(b_2^2)[C_{2v}] <$

**TABLE 2: Calculated$^a$ Line Positions and Intensities for the Photoelectron Spectrum of $Al_3O^-$**

| state | binding energy$^b$ (eV) | intensity$^c$ ($S_j^2$) | important configurations$^d$ |
|---|---|---|---|
| $^2B_2$ | 1.68 | 0.89 | $0.93(3b_2)^{-1}$ |
| $^2A_1$ | 3.51 | 0.76 | $0.84(4a_1)^{-1}$; $0.30(3b_2)^{-2}(5a_1)^1$ |
| $^2B_2$ | 3.94 | 0.79 | $0.85(2b_2)^{-1}$; $0.21(3b_2)^{-1}(4a_1)^{-1}(5a_1)^1$ |
| $^2A_1$ | 4.61 | 0.15 | $0.73(3b_2)^{-2}(5a_1)^1$; $0.27(4a_1)^{-1}$ |
| $^2A_1$ | 5.22 | 0.56 | $0.71(3a_1)^{-1}$; $0.39(2b_2)^{-1}(3b_2)^{-1}(5a_1)^{-1}$; $0.26(3b_2)^{-2}(5a_1)^1$ |
| $^2A_1$ | 6.01 | 0.07 | $0.51(3b_2)^{-2}(8a_1)^1$; $0.36(3b_2)^{-2}(na_1)^1$; $0.24(3b_2)^{-2}(7a_1)^1$ |
| $^2B_1$ | 6.76 | 0.06 | $0.35(4a_1)^{-1}(3b_2)^{-1}(2a_2)^1$; $0.28(2b_2)^{-1}(3b_2)^{-1}(3b_1)^1$; $0.28(2b_2)^{-1}(3b_2)^{-1}(2b_1)^1$; $0.26(3b_2)^{-2}(2b_1)^1$ |
| $^2B_1$ | 6.81 | 0.76 | $0.86(1b_1)^{-1}$ |
| $^2A_1$ | 7.73 | 0.07 | $0.43(2b_2)^{-1}(3b_2)^{-1}(5a_1)^1$; $0.28(4a_1)^{-2}(5a_1)^1$; $0.21(3a_1)^{-1}$ |
| $^2A_1$ | 8.07 | 0.25 | $0.49(2a_1)^{-1}$; $0.41(4a_1)^{-2}(5a_1)^1$; $0.28(2b_2)^{-2}(5a_1)^1$ |
| $^2A_1$ | 8.18 | 0.10 | $0.37(2b_2)^{-1}(3b_2)^{-1}(5a_1)^1$; $0.35(3b_2)^{-2}(na_1)^1$; $0.30(3b_2)^{-2}(n'a_1)^1$ |
| $^2A_1$ | 8.65 | 0.31 | $0.50(2a_1)^{-1}$; $0.31(2b_2)^{-2}(5a_1)^1$; $0.30(2b_2)^{-1}(3b_2)^{-1}(5a_1)^1$ |
| $^2B_2$ | 9.74 | 0.06 | $0.38(3b_2)^{-1}(3a_1)^{-1}(5a_1)^1$; $0.27(2b_2)^{-1}(4a_1)^{-1}(5a_1)^1$ $0.24(1b_2)^{-1}$; $0.23(3a_1)^{-1}(2b_2)^{-1}(5a_1)^1$ |

$^a$ For each symmetry, the $2h-1p$ wave functions were used for the anion and neutral molecule. The transitions from $^1A_1$ state of $Al_3O^-$ ($C_{2v}$) have been considered. $^b$ The first $^2B_2$ state energy was adjusted to experimental data (1.68 eV) and the same constant shift used for all other states. $^c$ The values less than 0.05 were not listed. $^d$ The absolute values for the CI coefficients were taken. All molecular orbitals of higher energy than $8a_1$ were denoted as $na_1$ or $n'a_1$.

$^3A_2'$ $(a_1^1 b_1^1)[D_{3h}] < {}^1A_1(a_1^2)$ $[C_{2v}] < {}^1B_2$ $(a_1^1 b_1^1)[C_{2v}]$. With the TCSCF method, the difference in energy between the global minimum singlet and triplet structures (i.e., $^1A_1(b_2^2)[C_{2v}]$ and $^3A_2'$ $(e'^2)[D_{3h}]$) is small (2.2 kcal/mol) compared to UB3LYP (10.5 kcal/mol), UCCD (6.7 kcal/mol), and UCCSD(T) (9.8 kcal/mol) methods.

In Table 2 we have reported the results of $2h-1p$ CI calculations for different excited states of $Al_3O$. Here only the vertical transitions from the $^1A_1$ $(b_2^2)[C_{2v}]$ minimum of $Al_3O^-$ to various states of $Al_3O$ have been considered. The energy of all roots has been shifted by a constant so the lowest energy root ($^2B_2$) agrees with the corresponding 1.68 eV vertical ionization peak in the experimental spectrum. For the negative ion of $Al_3O^-$ ($^1A_1$ state) a small CI calculation was done and, using both the negative ion wave function and neutral wave functions, pole strength values were calculated for different states. In addition to the binding energies, this Table 2 also includes the calculated pole strength values ($S_j^2$) and the leading terms in the wave function for each state. For each symmetry the lowest 20 roots are considered and only those states whose calculated pole strength value is greater than 0.05 have been listed in the table. From Table 2 it can be seen that the primary hole states associated with ionization from the $3b_2$, $4a_1$, $2b_2$, $3a_1$, and $1b_1$ orbitals can be easily identified. It is harder to identify the primary or parent hole states corresponding to the ionization of the $2a_1$ or $1a_1$ orbitals since the CI coefficients for these configurations are small in all states due to the high correlation effects.

If one considers only the allowed transitions from the $^1A_1$ state of $Al_3O^-$ to different states of neutral $Al_3O$, all the features in the experimental spectrum cannot be explained. In order to

**TABLE 3: Calculated[a] Line Positions and Intensities for the Photoelectron Spectrum of Al₃O⁻**

| state | binding energy[b] (eV) | intensity[c] ($S_j^2$) | important configurations[d] |
|---|---|---|---|
| $^2E'$ | 1.22 | 0.91 | $0.94(3e')^{-1}$ |
| $^4E'$ | 3.30 | 1.03 | $0.87(2e')^{-1}; 0.21(2e')^{-1}(3e')^{-1}(4e')^1$ |
| $^2E'$ | 3.77 | 0.12 | $0.87(2e')^{-1}; 0.22(2a_1')^{-1}(3e')^{-1}(4e')^1$ |
| $^2E'$ | 4.23 | 0.26 | $0.76(2e')^{-1}; 0.41(2a_1')^{-1}$ |
| $^4A_2'$ | 4.59 | 0.90 | $0.84(2a_1')^{-1}; 0.37(2e')^{-1}(3e')^{-1}(4e')$ |
| $^2E'$ | 5.35 | 0.19 | $0.69(2e')^{-1}; 0.36(2a_1')^{-1};$ $0.25(2e')^{-1}(3e')^{-1}(4e')^1$ |
| $^2A_2'$ | 6.70 | 0.05 | $0.723(2e')^{-2}(3e')^1;$ $0.40(2a_1')^{-1}(2e')^{-1}(3e')^1; 0.28(2a_1')^{-1}$ |
| $^4A_1''$ | 6.80 | 1.10 | $0.90(1a2'')^{-1}$ |
| $^2A_1''$ | 6.90 | 0.55 | $0.90(1a2'')^{-1}$ |
| $^2A_2'$ | 7.02 | 0.42 | $0.77(2a_1')^{-1}; 0.20(2a_1')^{-1}(2e')-1(3e')^1$ |
| $^4E'$ | 8.37 | 0.17 | $0.36(1e')^{-1}; 0.30(2e')^{-1}(3e')^{-1}(5e')^1;$ $0.23(2e')^{-1}(3e')^{-1}(4e')^1$ |
| $^4A_2'$ | 8.63 | 0.11 | $0.63(2e')^{-1}(3e')^{-1}(4e')^1; 0.29(2a_1')^{-1}$ |
| $^4E'$ | 8.67 | 0.35 | $0.53(1e')^{-1}; 0.32(2a_1')^{-1}(3e')^{-1}(4e')^1$ |
| $^4E'$ | 9.39 | 0.18 | $0.36(1e')^{-1}; 0.36(2e')^{-2}(4e')^1;$ $0.29(2e')^{-1}(3e')^{-1}(na_1')^1$ |
| $^4A_1'$ | 9.58 | 0.05 | $0.42(2e')^{-1}(3e')^{-1}(na_1')^1;$ $0.24(2a_1')^{-1}(3e')^{-1}(na_1')^1$ $0.28(2e')^{-1}(3e')^{-1}(n'a_1')^1$ |

[a] For each symmetry, the $2h-1p$ wave functions were used for the anion and neutral molecule. The transitions from the $^3A_2'$ state of Al₃O⁻ ($D_{3h}$ symmetry) have been considered. [b] The first $^2E'$ state energy was adjusted to experimental data (1.22 eV) and the same constant shift used for all other states. [c] The values less than 0.05 were not listed. For quartet states calculated $S_j^2$ values were multiplied by a factor of 4/3 due to symmetry reason. [d] The absolute values for the CI coefficients were taken. All molecular orbitals of higher energy than $2a_1'$ were denoted as $na_1'$ or $n'a_1'$.

test whether there might be transitions originating from the $^3A_2'$ state of Al₃O⁻ to different states of Al₃O, we have calculated the vertical binding energies and pole strength values for those transitions also. In Table 3 we have presented the results using the $^3A_2'$ state geometry ($D_{3h}$ symmetry) of Al₃O⁻ in the calculation of the Dyson orbital. Similar to the calculations using $^1A_1$ geometry, we have calculated 20 roots for each symmetry states of neutral Al₃O and the ground state for Al₃O⁻. Since energetically the $^3A_2'$ state has been found to be slightly higher than the $^1A_1$ state, we have assumed that the lowest energy peak with very small intensity in the observed photoelectron spectrum of Al₃O⁻ is probably a hot band due to the transition from the $^3A_2'$ state of Al₃O⁻ to the ground state of Al₃O. On the basis of this, we have adjusted the lowest energy transition from this calculation using the $^3A_2'$ geometry to match the low intensity 1.22 eV vertical ionization peak of the spectrum. All other binding energies have been shifted by the same constant. In this table, the states having pole strength values 0.05 or larger have been reported. From this table it can be seen that the low-energy primary hole states are mainly due to the ionization from $3e'$, $2e'$, $2a_1'$, and $1a_2''$ orbitals. All other states are $2h-1p$ states.

The next level of calculation was MRSDCI calculations for the lowest few roots of the CI matrix of each symmetry to cover the range up to binding energies of approximately 8 eV. For each symmetry, the dominant configurations from the $2h-1p$ CI calculations (coefficient greater than 0.05) were used as the reference space and perturbation theory was used to select approximately 120 000 to 170 000 configurations for each symmetry. MRSDCI calculations were done for both $^1A_1$ and $^3A_2'$ geometries. Similarly for the negative ion of Al₃O, MRSDCI calculations provided the ground-state wave function for computing the Dyson orbitals and the corresponding pole strength. The calculated negative ion ground states energies were
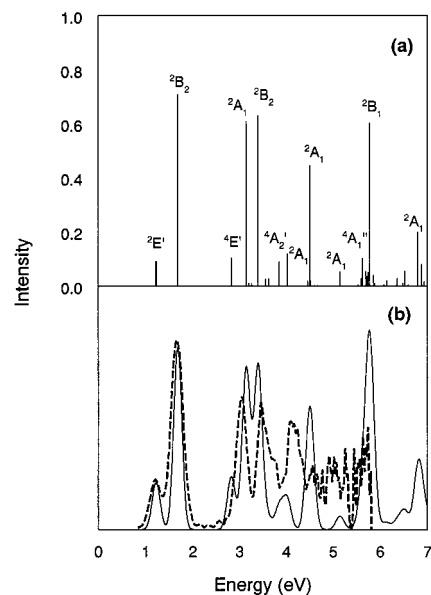


**Figure 3.** (a) Theoretical spectrum obtained using the calculated energies and pole strength values from $2h-1p$ calculations. The energies have been shifted and scaled to make the first two peaks agree with experiment. (b) Comparison between the experimentally observed and theoretically derived photoelectron spectrum of Al₃O⁻. The dashed line represents the experimental spectrum and solid line represents the theoretically simulated spectrum.
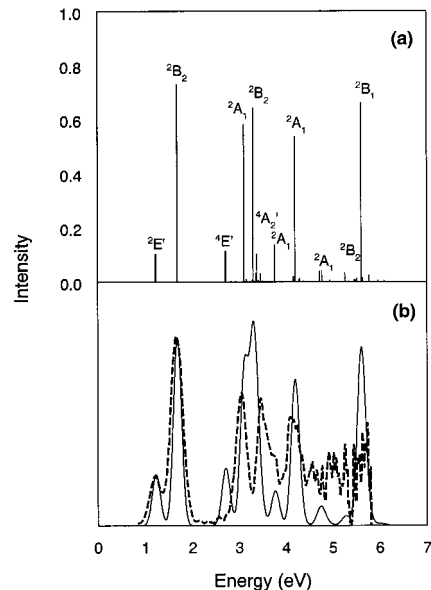


**Figure 4.** (a) Theoretical spectrum obtained using the calculated energies and pole strength values from MRSDCI calculations. The peaks have been shifted and scaled to make the first two peaks agree with experiment (b) Comparison between the experimentally observed and theoretically derived photoelectron spectrum of Al₃O⁻. The dashed line represents the experimental spectrum and solid line represents the theoretically simulated spectrum.

−801.054 371 and −801.053 557 au for the $^1A_1$ and $^3A_2'$ states, respectively.

Our best interpretation of the binding energy spectrum of Al₃O⁻ using the $2h-1p$ and MRSDCI results obtained in the present work have been reported in Figures 3 and 4, respectively. In these plots, the energy differences from the lowest peak have been scaled to agree with the next peaks and the remaining energy differences have been scaled by the same factor. Qualitatively, both of the calculated spectra are similar. The peak positions and intensities corresponding to the line spectrum

of Figures 3a and 4a have been utilized to generate a pseudo-spectrum, based on equal width Gaussians with heights proportional to the calculated weights, and are plotted as Figures 3b and 4b, respectively. For the purpose of comparison, the experimental spectra[18] are plotted in Figures 3b and 4b as dashed lines. It is interesting to note that after exact matching of the first two calculated peaks with the experiment, the calculated peak positions and intensities for the rest of the spectrum are found to agree very well with the experimental spectrum considering that no transition moment factors and no vibrational effects have been included.

In the calculated spectrum, the very low intensity features shown in the stick spectrum of Figures 3a and 4a are not visible in the smoothed spectrum in Figures 2b and 3b due to the Gaussian widths of the more intense peaks. On the basis of the present theoretical results, it is evident that there are two different geometries ($^1A_1$ and $^3A_2'$ state) of the negative ion of $Al_3O$ involved in the photoelectron spectrum. The very first low intensity peak was not assigned to any electronic state by Wu et al. In our results, it is assigned as $(3e')^{-1}\ ^2E' \leftarrow\ ^3A_2'$. There is no ambiguity regarding the second peak which has been correctly assigned by Wu et al. as $(3b_2)^{-1}\ ^2B_2 \leftarrow\ ^1A_1$. The third peak, which was assigned by Wu et al. as $A\ ^2B_1 \leftarrow\ ^1A_1$ on the basis of the typing error in the Boldyrev and Schleyer paper,[13] has been found to be $(4a_1)^{-1}\ ^2A_1 \leftarrow\ ^1A_1$. Some low-energy satellite structure between the second and third peak (not assigned by Wu et al.) is due to the $(2e')^{-1}\ ^4E' \leftarrow\ ^3A_2'$ transition. The fourth peak, which was previously assigned as $^2A_1$, has been found to be $(2b_2)^{-1}\ ^2B_2 \leftarrow\ ^1A_1$ in our assignment. After the fourth peak position, there are some shoulders which we find to be due to the $(2a_1')^{-1}\ ^4A_2' \leftarrow\ ^3A_2'$ and $(3b_2)^{-2}(5a_1)^1\ ^2A_1 \leftarrow\ ^1A_1$ transitions. The fifth peak has been assigned as $(3a_1)^{-1}\ ^2A_1 \leftarrow\ ^1A_1$ by both us and Wu et al. The photoelectron peaks around 5 eV energy were not well resolved experimentally and were not assigned to any transition. We predict that these are due to low-intensity satellites originating from $^1A_1$ as well as a $(1a_2')^{-1}\ ^4A_1'' \leftarrow\ ^3A_2'$ primary hole transition. At around 5.8 eV energy, we expect intensity due to the $(1b_1)^{-1}\ ^2B_1 \leftarrow\ ^1A_1$ transition.

## Summary

The equilibrium geometries of the low lying electronic states of $Al_3O$ and $Al_3O^-$ have been calculated using CASSCF, UB3LYP, and CCD levels of theory. Within the $C_{2v}$ symmetry, the calculated global minimum for $Al_3O$ and $Al_3O^-$ were found to be $^2B_2$ and $^1A_1$ with respective highest occupied molecular orbital occupations $(3b_2)^1$ and $(3b_2)^2$. The $^3A_2'$ state of $Al_3O^-$ was found to have $D_{3h}$ symmetry and slightly higher energy than the corresponding $C_{2v}$ symmetry $^1A_1$ state. It has been found that the $^1A_1$ configuration $(5a_1)^2$, the $^1B_2$ configuration $(3b_2)^1$-$(5a_1)^1$ and $^2A_1$ with a $(5a_1)^1$ configuration are all transition states on the respective potential energy surfaces for pseudorotation. Using the calculated geometries of $Al_3O^-$ at CCD level of theory, configuration interaction (CI) calculations have been done to determine the low-lying vertical excited states of $Al_3O$, and those results have been utilized to interpret the recently reported experimental photoelectron spectrum of $Al_3O^-$. Some of the previous assignments for the photoelectron peaks in the observed spectrum were found to be incorrect and new assignments have been made for those peaks.

## References and Notes

(1) See, for example: Desjardins, S. J.; Bawagan, A. D. O.; Liu, Z. F.; Tan, K. H.; Yang, Y.; Davidson, E. R. *J. Chem. Phys.* **1995**, *102*, 6385, and references therein.

(2) Bawagan, A. D. O.; Desjardins, S. J.; Dailey, R.; Davidson, E. R. *J. Chem. Phys.* **1997**, *107*, 4295.

(3) Moghaddam, M. S.; Desjardins, S. J.; Bawagan, A. D. O.; Tan, K. H.; Yang, Y.; Davidson, E. R. *J. Chem. Phys.* **1995**, *103*, 10537.

(4) Rolke, J.; Zheng, Y.; Brion, C. E.; Yang, Y. A.; Davidson, E. R. *Chem. Phys.* **1998**, *230*, 153.

(5) Bawagan, A. D. O.; Ghanty, T. K.; Davidson, E. R.; Tan, K. H. *Chem. Phys. Lett.* **1998**, *287*, 61.

(6) Ghanty, T. K.; Davidson, E. R. *Mol. Phys.*, in press.

(7) Cederbaum, L. S.; Domcke, W.; Schirmer, J.; von Niessen, W. *Adv. Chem. Phys.* **1986**, *65*, 115.

(8) *Metal Clusters*; Moskovits, M., Ed.; Wiley: New York, 1986.

(9) *Physics and Chemistry of Small Clusters*; Jena, P., Rao, B. K., Kanna, S. N., Eds.; NATO Advanced Science Institutes Series 158; Plenum: New York, 1987.

(10) Cox, D. M.; Trevor, D. J.; Whitten, R. L.; Rohling, E. A.; Kaldor, A. J. *J. Chem. Phys.* **1986**, *84*, 4651.

(11) Kudo, H. *Nature* **1992**, *355*, 432.

(12) Wang, S. L.; Ledingham, K. W. D.; Singhal, R. P. *J. Phys. Chem.* **1996**, *100*, 11282.

(13) Boldyrev, A. I.; Schleyer, P. v. R. *J. Am. Chem. Soc.* **1991**, *113*, 9045.

(14) Boldyrev, A. I.; Shamovsky, I. L.; Schleyer, P. v. R. *J. Am. Chem. Soc.* **1992**, *114*, 6469.

(15) Vyacheslav, V. G.; Niessen, W. v.; Boldyrev, A. I.; Schleyer, P. v. R. *Chem. Phys.* **1993**, *174*, 167.

(16) Boldyrev, A. I.; Simons, J.; Zakrzewski, V. G.; Niessen, W. v. *J. Phys. Chem.* **1994**, *98*, 1427.

(17) Schleyer, P. v. R.; Kapp, J. *Chem. Phys. Lett.* **1996**, *255*, 363.

(18) Wu, H.; Li, X.; Wang, X. B.; Ding, C. F.; Wang, L. S. *J. Chem. Phys.* **1998**, *109*, 449.

(19) *Gaussian 94*; Frisch, M. J.; Trucks, G. W.; Schlegel, H. B.; Gill, P. M. W.; Johnson, B. G.; Robb, M. A.; Cheeseman, J. R.; Keith, T. A.; Peterson, G. A.; Montgomery, J. A.; Raghavachari, K.; Al-Laham, M. A.; Zakrzewski, V. G.; Ortiz, J. V.; Foresman, J. B.; Cioslowski, J.; Stefanov, B. B.; Nanayakkara, A.; Challacombe, M.; Peng, C. Y.; Ayala, P. Y.; Chen, W.; Wong, M. W.; Andres, J. L.; Replogle, E. S.; Gomperts, R.; Martin, R. L.; Fox, D. J.; Binkley, J. S.; Defrees, D. J.; Baker, J.; Stewart, J. P.; Head-Gordon, M.; Gonzalez, C.; Pople, J. A. Gaussian, Inc., Pittsburgh, PA, 1995.

(20) Dupuis, M.; Marquez, A.; Davidson, E. R. "HONDO 95.6", IBM Corp., Neighborhood Road, Kingston, NY 12401, 1995.

(21) MELD is a set of electronic structure programs written by McMurchie, L. E.; Elbert, S. T.; Langhoff, S. R.; Davidson, E. R., with extensive modifications by Feller, D.; Rawlings, D. C.

(22) Dunning, T. H., Jr. *J. Chem. Phys.* **1989**, *90*, 1007. Woon, D. E.; Dunning, T. H., Jr. *J. Chem. Phys.* **1993**, *98*, 1358. Kendall, R. A.; Dunning, T. H., Jr.; Harrison, R. J. *J. Chem. Phys.* **1992**, *96*, 6769. Basis sets were obtained from the Extensible Computational Chemistry Environment Basis Set Database, Version 1.0, as developed and distributed by the Molecular Science Computing Facility, Environmental and Molecular Sciences Laboratory, which is part of the Pacific Northwest Laboratory, P.O. Box 999, Richland, WA 99352, and funded by the U.S. Department of Energy. The Pacific Northwest Laboratory is a multiprogram laboratory operated by Battelle Memorial Institute for the U.S. Department of Energy under contract DE-AC06-76RLO 1830. Contact David Feller, Karen Schuchardt, or Don Jones for further information.

(23) Feller, D.; Davidson, E. R. *J. Chem. Phys.* **1981**, *84*, 3977.

(24) Davidson, E. R. *J. Am. Chem. Soc.* **1977**, *99* 397.

(25) Pearson, R. G. *J. Am. Chem. Soc.* **1969**, *91*, 4947. Borden, W. T.; Davidson, E. R.; Hart, P. *J. Am. Chem. Soc.* **1978**, *100*, 388.